atoms

MDPI

Article

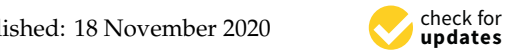
Study of Electron and Positron Elastic Scattering from Hydrogen Sulphide Using Analytically Obtained Static Potential

Dibyendu Mahato, Lalita Sharma * and Rajesh Srivastava

Department of Physics, Indian Institute of Technology, Roorkee 247667, India; dmahato@ph.iitr.ac.in (D.M.); rajesh.srivastava@ph.iitr.ac.in (R.S.)

* Correspondence: lalita.sharma@ph.iitr.ac.in

Received: 22 October 2020; Accepted: 16 November 2020; Published: 18 November 2020



Abstract: A detailed study of elastic scattering of electrons and positrons from a hydrogen sulphide (H_2S) molecule is presented using the method of partial wave phase shift analysis with suitably chosen complex optical potentials. The important aspect of our present work is that we uniquely obtain static potential in an analytical form and use it along with exchange (only for electron), polarization and purely imaginary absorption potentials to define the complex optical potential. The static potential is evaluated by obtaining charge density from the H_2S molecule using the molecular wavefunction represented through an accurate analytical form of the Gaussian orbitals. The primary aim of our study is to test our present approach, as applied to the electron and positron scattering from H_2S. Therefore, the results for electron and positron impact differential, integral, momentum-transfer, absorption and total cross sections are obtained for the incident energies in the range of 10–500 eV. Comparisons of these different types of cross section results with the available measurements and other calculations show good agreement, which suggests the applicability of our present approach.

Keywords: electron–positron scattering; static potential; Gaussian wavefunction; complex optical potential; cross sections

1. Introduction

Electron- and positron-molecule elastic scattering processes are important in understanding their transport and drift in any molecular medium as well as their interaction with electrons and nuclei present in the molecule. One common way to study such a process is using the method of partial wave phase shift analysis with complex optical potential which is usually expressed in terms of static, exchange (for electron), polarization and purely imaginary absorption potentials. The study of electron impact is different from that of positron impact, mainly in the sense that the static potentials seen by them with respect to molecular targets are, respectively, attractive and repulsive. Since a positron is distinguishable from the target electrons, the exchange potential must be dropped for positron scattering studies. However, the polarization potential is attractive for both the electron and positron scattering. Thus, it would be interesting for the current research to study both the electron and positron scattering from any important molecule. In the case of inelastic scattering of the positron, the positronium formation channel opens, in addition to excitation and ionization. Positronium is short-lived when it is produced and is annihilated by combining with an electron to form gamma rays, so the study of electron and positron scattering from astrophysical molecules is an interesting topic for the current research. In the present work, we focus on the analysis of elastic electron and positron scattering from hydrogen sulphide by taking a suitably defined complex optical potential, where we use our uniquely obtained analytical form of the static potential.

The study of H_2S is of great significance as it is a quasi-spherical symmetric molecule and commonly found in most of the astrophysical environments, such as in interstellar space and on the comet Austin (1989C1) [1]. Recent evidence of the clear detection of gaseous H_2S above the Uranus cloud deck has been noticed at a pressure level of between 1.2 bar and 3 bar [2] and it is expected that H_2S is the main sulphur hydride found in dense clouds. H_2S is also detected in the proto-planetary disks of GG Tau A [3] and hence, to characterize the properties and initial conditions of planet formation, we need to study the molecular species present in it. In the astronomical environment, positron annihilation gamma rays originate from solar flares [4] towards the Milky Way [5]. The detection of such rays gives us vital information about the solar system and the surrounding environment. Thus, the presence of H_2S has been clearly observed in different astrophysical environments. Besides the astrophysical environments, highly polar H_2S has been very active in chemical reactions where it has been used in a large number of chemical and physical processes [6]. H_2S is also an essential biological gas transmitter in health and diseases [7], as well as being used to develop drugs for cardiovascular disease [8]. The electron impact processes also play various roles in biomedical applications such as modeling software [9–11] to estimate radiation-induced damage in biological systems. In addition, H_2S is also used in plasma nitro-carburizing processes along with N_2 and H_2 [12] and hence, to understand and characterize such a plasma, the electron scattering cross sections from H_2S are required.

Before we discuss our method to study electron/positron scattering from H_2S, it is worth giving a brief review of the available experimental and theoretical work undertaken so far. Many studies have reported elastic scattering cross sections in the different ranges viz. low, intermediate, and high incident electron energies. Gulley et al. [13] measured the differential cross sections (DCS), integrated cross sections (ICS), and momentum transfer cross sections (MTCS) for incident electron energy from 1–30 eV using a crossed electronic-molecular beam apparatus with an angular variation of 20°–130°. Similarly, with the addition of the relative flow technique, Rawat et al. [14] measured the cross sections in the energy range of 100–500 eV through 10°–140° angular distributions. Further, the most recent experiments on e-H_2S cross sections have been reported by Cho et al. [15] and Brescansin et al. [16] in the energy range 3–30 eV and 30–100 eV, respectively, over the scattering angle 10°–180° with a crossed-beam electron spectrometer combined with a magnetic angle-changing device. Besides experimental work, several previous theoretical calculations have been completed, for instance, Rawat et al. [14] reported DCS, ICS, MTCS in the energy range from 0.5–500 eV using the Schwinger variational method combined with the distorted-wave approximation. A modified similar approach has been used by Brescansin et al. [16] to calculate the DCS, ICS, and MTCS in the energy range of 1 to 500 eV. Varella et al. [17] performed their calculation in between 5–30 eV energy, using a Schwinger multichannel method with pseudo-potentials, along with a Born closure procedure in order to account for the long-range potential of the targets. Machado et al. [18] calculated DCS in the range of 2–50 eV using fixed-nuclei and static-exchange approximations for the low partial-wave scattering amplitudes via the Schwinger variational iterative method, whereas, Born approximation with a point-dipole potential was used to account for higher partial waves. Jain et al. [19] performed calculations for 50–1000 eV by constructing an optical potential from a near Hartree–Fock one-center expansion. Gianturco et al. [20] calculated the DCSs up to 25 eV by using the single center expansion method. Yuan and Zhang [21] performed the DCS, TCS and MTCS calculations from 0.1–50 eV within the Born–Oppenhermer approximation. Nishimura and Itikawa [22] employed a close-coupling method to determine the ab initio electrostatic potential and reported DCSs from 3–30 eV. Gupta and Baluja [23] obtained DCS results from 3–15 eV by using the R-matrix method. Further, Aouchiche et al. [24] reported DCSs and ICSs in a wide range of energy from 10–1000 eV. They used partial wave formalism with a spherically symmetric complex optical potential, where the static contribution was deduced from a single center Hartree–Fock target description. For the total absorption cross section (ACS) only the theoretical calculations by Brescansin et al. [16] and Jain and Baluja [25] are available; both of them use a quasi-free spherical model. On the other hand, Szmytkowsky et al. [26] reported the total cross section (TCS) results from 6–370 eV using a modified electron spectrometer working in a linear transmission mode.

Zecca et al. [27] performed TCS measurements on a Ramsauer-type apparatus for electron scattering in the energy range from 5–4000 eV. There are a couple of theoretical calculations available for TCS, such as from Brescansin et al. [16], Jain and Baluja [25] and Joshipura and Vinodkumar [28] and Limbachiya et al. [29]. For positron scattering from H_2S, there are no earlier experimental or theoretical studies reported. However, such studies can be equally important to probe the nature of positron–H_2S interactions, as well as to compare with similar electron impact results.

As mentioned earlier, most of the electron-molecule elastic scattering has been studied with the optical potential approach using the partial wave phase shift analysis with suitably chosen complex optical potential, which consists of the static potential along with the exchange, polarization and imaginary absorption potentials. The entire complex optical potential is then used in the Schrödinger equation [30–32] which is solved by partial wave phase shift analysis to obtain the scattering cross sections. As one can see from the review given above, this approach is quite successful and has been widely applied in studying the elastic scattering of electrons with different atoms and molecules, including H_2S. However, various optical potential choices make a real difference in the accuracy of the results obtained from such an approach. For example, evaluating the target molecule's static potential as seen by the projectile electron or positron is an arduous and challenging task for a multicenter target [33,34], as one needs to correlate interactions between all the individual atoms and the projectile. There are many methods available that have been used in the past to obtain the multicenter molecular potentials. The single-center expansion (SCE) method [35] is one of the most widely implemented approaches in which wavefunction of the molecular orbitals are expanded with respect to the center of mass of a polyatomic molecule and numerical integration is used to obtain the potentials. Whereas, we have developed a method which obtains the spherically-averaged static potential by evaluating multicenter integrals using Gaussian orbitals centered on the various nuclei. It is worth mentioning here that our static potential is mostly analytic, except for the inclusion of the well-known error functions, which is advantageous due to available algorithms for their numerical evaluation. Thus, the accuracy of our potential is dependent only on the reliability of the Gaussian wavefunctions that we have used to represent the molecule. In fact, we have used STO-6G Gaussian wavefunctions in this work, which are quite accurate. For other potentials viz. exchange, polarization and absorption components of the complex optical potential, we have used standard and widely tested expressions [36–41]. Here, one of our main aims is to test our method for obtaining the static potential as applied to e-H_2S scattering by comparing our calculated DCS, ICS, MTCS, ACS and TCS results with the available measurements and other calculations. This will provide us the confidence to extend the applications of the present method to study scattering from other complex molecules in a similar way. We further utilize the method to report similar cross section results for the elastic collision of positrons with H_2S and compare these with electron impact results.

In Section 2, we briefly describe the theoretical method to obtain the static potential and different cross sections. Thereafter, our calculated results are presented and compared with other theoretical and experimental results in Section 3.

2. Theory

2.1. Scattering Amplitude and Cross Sections

The scattering of electrons and positrons from a small molecule like H_2S can be described in a non-relativistic manner by the Schrödinger equation as given below [30] (atomic units are used throughout)

$$\left[\frac{1}{2}\nabla^2 + E - V_{opt}\right]\Psi(\boldsymbol{r}) = 0. \tag{1}$$

Here, E refers to the incident electron or positron energy, $\Psi(\boldsymbol{r})$ is the wavefunction and $V_{opt}(r)$ is the total complex optical potential, which includes static $V_{st}(r)$, exchange $V_{ex}(r)$, polarisation $V_{pol}(r)$ and absorption $V_{abs}(r)$ potentials for electron, i.e.,

$$V_{opt}(r) = V_{st}(r) + V_{ex}(r) + V_{pol}(r) + iV_{abs}(r). \tag{2}$$

In the case of positron scattering, the exchange potential needs to be dropped, as already explained earlier. The choices of these potentials have been discussed in detail in the following Section 2.2. Although H_2S is a quasi-spherically symmetric molecule with heavier atom S at the center, the interaction potential $V_{opt}(r)$ is approximated as spherically symmetric. Further, to study the elastic scattering of an electron or a positron from H_2S molecule, we consider it a rigid non-rotating system and exclude any rotational excitation contribution of the molecule in our present calculations.

By expanding the wavefunction $\Psi(\boldsymbol{r})$ in terms of its partial waves and phase shifts in the usual standard manner and then substituting in Equation (1), we obtain the following radial equation

$$\left(\frac{d^2}{dr^2} + k^2 - 2V_{opt}(r) - \frac{l(l+1)}{r^2}\right)u_l(r) = 0, \tag{3}$$

where $k^2 = 2E$, k is the momentum of electron or positron and $u_l(r)$ is the radial wavefunction associated with partial wave l satisfying Equation (3) and can be solved subjecting to the following asymptotic boundary conditions,

$$u_l(r) \sim \frac{1}{k}\sin\left(kr - \frac{l\pi}{2} + \delta_l\right), \text{ for } r \to \infty \text{ and } u_l(r) \sim 0 \text{ for } r \to 0. \tag{4}$$

Here, $\delta_l = \delta_{Real} + i\delta_{abs}$ is the complex phase shift of l^{th} outgoing partial wave with respect to the free spherical wave in the presence of the potential. Further, the solution of Equation (3) gives us the phase shift at each kinetic energy of the incident electron [30,31], in terms of which we can express the scattering amplitude by the following expression,

$$f(\theta) = \frac{1}{2ik}\sum_{l=0}^{\infty}(2l+1)\left(e^{2i\delta_l} - 1\right)P_l(\cos\theta), \tag{5}$$

where $P_l(\cos\theta)$ is the l^{th} order Legendre polynomial. $\left|f(\theta)\right|^2$ gives differential cross section, while total elastic integral (σ_{el}), momentum transfer cross section (σ_{mtcs}) and absorption cross sections (σ_{abs}) are finally obtained by using the following expressions [30,31,42]

$$\sigma_{el} = \frac{\pi}{k^2}\sum_{l=0}^{\infty}(2l+1)\left|1 - e^{2i\delta_l}\right|^2, \tag{6}$$

$$\sigma_{mtcs} = \frac{4\pi}{k^2}\sum_{l=0}^{\infty}(l+1)\sin^2(\delta_{l+1} - \delta_l) \tag{7}$$

and,

$$\sigma_{abs} = \frac{\pi}{k^2}\sum_{l=0}^{\infty}(2l+1)\left[1 - \left|e^{-2Im\delta_l}\right|^2\right]. \tag{8}$$

Further, the total cross section (σ_{total}) is obtained by adding the total elastic integrated cross section (σ_{el}) with the absorption cross section (σ_{abs}).

2.2. Complex Optical Potential

To solve Equation (3), we first need to construct an appropriate complex optical potential by properly defining its different component potentials as given in Equation (2). Out of these component potentials the calculation of the static potential is quite nontrivial and of fundamental importance in the present work. We first calculate the charge density of H_2S molecule by taking the squared modulus of the molecular wavefunction at a point $\boldsymbol{r}'$ as seen by the projectile.

$$\rho(\boldsymbol{r}') = \sum_i \left|X_i(\boldsymbol{r}')\right|^2, \tag{9}$$

where X_i is the molecular wavefunction of the i^{th} molecular orbital and here i sum over the number of molecular orbitals, which are 9 for H_2S. The molecular orbitals $X_i(\boldsymbol{r}')$ are further expressed as linear combination of atomic orbitals $\phi_k(\boldsymbol{r}')$, i.e.,

$$X_i(\boldsymbol{r}') = \sum_k a_{ik}\phi_k(\boldsymbol{r}'), \tag{10}$$

here a_{ik} is the molecular orbital co-efficient and k extends on the total number of atomic orbitals, which are 11 for H_2S. Each atomic orbital is represented as

$$\phi_k(\boldsymbol{r}') = \sum_j N_{kj}c_{kj}\chi_{kj}(\boldsymbol{r}'), \tag{11}$$

where N_{kj} and c_{kj} are the normalization constants and coefficients of the Gaussian basis functions $\chi_{kj}(\boldsymbol{r}')$, respectively. The sum over j denotes the number of Gaussian basis function. Thus, by combining Equations (10) and (11) with Equation (9), the total charge density can be expressed in the following general form as,

$$\rho(\boldsymbol{r}') = \sum_i \sum_{k,k'} a_{ik}a_{ik'} \sum_{j,j'} N_{kj}N_{k'j'}c_{kj}c_{k'j'}\chi_{kj}(\boldsymbol{r}')\chi_{k'j'}(\boldsymbol{r}'). \tag{12}$$

Here, the unnormalized form of the Gaussian basis function $\chi_{kj}(\boldsymbol{r}')$, which is centered on its nucleus **A** with coordinates A_x, A_y and A_z can be represented as

$$\chi_{kj}(\boldsymbol{r}') = e^{-\alpha_{kj}|\boldsymbol{r}'-\mathrm{A}|^2}(x'-A_x)^{m_x}\Big(y'-A_y\Big)^{m_y}(z'-A_z)^{m_z}, \tag{13}$$

Here, m_x, m_y and m_z are non-negative integers and α_{kj} are the exponents of the Gaussian basis function. To expand Equation (12) further, we used the important property of Gaussian orbitals, i.e., the product of the exponential parts of two Gaussian orbitals with different centers **A** and **B** can be written as an exponential of the same form at a center **P** on the line joining **A** and **B**. Thus, the product of two Gaussian functions in the expression of Equation (12) becomes

$$\begin{aligned}\chi_{kj}(\boldsymbol{r}')\chi_{k'j'}(\boldsymbol{r}') &= e^{-\alpha_{kj}|\boldsymbol{r}'-\boldsymbol{A}|^2}e^{-\alpha_{k'j'}|\boldsymbol{r}'-\boldsymbol{B}|^2}\\ &\times(x'-A_x)^{m_x}(y'-A_y)^{m_y}(z'-A_z)^{m_z}\\ &\times(x'-B_x)^{m'_x}(y'-B_y)^{m'_y}(z'-B_z)^{m'_z}\\ &= E_{kj,k'j'}e^{-\alpha|\boldsymbol{r}'-r_P|^2}(x'-A_x)^{m_x}\\ &\times(y'-A_y)^{m_y}(z'-A_z)^{m_z}\\ &\times(x'-B_x)^{m'_x}(y'-B_y)^{m'_y}(z'-B_z)^{m'_z},\end{aligned} \tag{14}$$

where $\boldsymbol{r}_P$ is the position vector of **P** with respect to the molecular frame can be given by

$$\boldsymbol{r}_P = \frac{\alpha_{kj}\mathbf{A} + \alpha_{k'j'}\mathbf{B}}{\alpha_{kj}+\alpha_{k'j'}},$$

and α and $E_{kj,k'j'}$ can be expressed as,

$$\alpha = \Big(\alpha_{kj}+\alpha_{k'j'}\Big)$$

and

$$E_{kj,k'j'} = e^{\left(-\frac{\alpha_{kj}\alpha_{k'j'}}{\alpha_{kj}+\alpha_{k'j'}}|\mathbf{A}-\mathbf{B}|^2\right)}.$$

Further, the electronic static interaction potential between a projectile electron and molecule at a point $\boldsymbol{r}$ can be represented by

$$V(r) = \int \frac{\rho(\boldsymbol{r}')}{|\boldsymbol{r}-\boldsymbol{r}'|}d\boldsymbol{r}'. \tag{15}$$

Now, expanding the denominator and using the property of spherical harmonics, we get the spherically averaged static potential over all the orientations of the molecule, i.e.,

$$V(r) = \sum_{i}\sum_{k,k'} a_{ik}a_{ik'}\sum_{j,j'} N_{kj}N_{k'j'}c_{kj}c_{k'j'}E_{kj,k'j'} \times \int e^{-\alpha|r'-r_p|^2}(x'-A_x)^{m_x}(y'-A_y)^{m_y}(z'-A_z)^{m_z} \times (x'-B_x)^{m'_x}(y'-B_y)^{m'_y}(z'-B_z)^{m'_z}\frac{1}{r_>}d\mathbf{r}', \quad (16)$$

here, the expression $r_>$ is greater of r and r'. Evaluation of the integrals in the above equation is conducted by considering the multiplications of the two different atomic Gaussian orbitals i.e., two s-orbital of hydrogen atoms (i.e., H (1s)) or say with s-orbital of Sulphur atom (i.e., S ($1s^2 2s^2 2p^6 3s^2 3p^4$)), s-orbital of H atom with the p-orbital of S atom and two p-orbitals of S atom. The integrals of Equation (16) for the interactions of s-s, s-p and p-p orbitals have been evaluated in terms of well-known error functions [43–45]. We have evaluated expression (Equation (16)) in a particular molecular frame of reference and this has been further discussed Section 3.

Further, to obtain the complete spherically averaged static potential, we have to take along with the electronic part of the static potential, the effective nuclear potential $V_{nucl}(r)$, which is expressed as,

$$V_{nucl}(r) = -\sum_{n=1}^{2}\frac{Z_{H_n}}{|\boldsymbol{r}-\boldsymbol{r}_{H_n}|} - \frac{Z_S}{|\boldsymbol{r}-\boldsymbol{r}_S|}. \quad (17)$$

Here, Z_{H_n} (n= 1–2 refers to two different hydrogen atoms of H_2S molecule) and Z_S are the atomic numbers of hydrogen and S atoms, respectively. Additionally, $\boldsymbol{r}_{H_n}$ and $\boldsymbol{r}_S$ are respective position vectors of the hydrogen atoms and S atom from the centre of mass of H_2S molecule. Thus, the total spherically-averaged static potential including the electronic as well as the nuclear charge distribution [46] for the H_2S molecules is

$$V_{st}(r) = V(r) - \frac{2Z_H}{r''_>} - \frac{Z_S}{r'''_>}. \quad (18)$$

Here, $r''_>$ is the maximum of (r, r_H) and $r'''_>$ is the maximum of (r, r_S). The total static potential for the electron-H_2S elastic scattering given by Equation (18) can be further simplified and expressed as [46,47]

$$V_{st}(r) = \begin{cases} V(r) - \frac{2Z_H}{r} - \frac{Z_S}{r} & \text{for } r \geq r_H. \\ V(r) - \frac{2Z_H}{r_H} - \frac{Z_S}{r} & \text{for } r_S < r < r_H. \\ V(r) - \frac{2Z_H}{r_H} - \frac{Z_S}{r_S} & \text{for } r \leq r_S. \end{cases} \quad (19)$$

Along with the static potential $V_{st}(r)$, we also include the exchange, polarisation and absorption potentials. We have chosen the modified exchange potential $V_{ex}(r)$ given by Gianturco and Scialla [36],

$$V_{ex}(r) = \frac{1}{2}\left[E - V_{st} + \frac{3}{10}\left(3\pi^2\rho(r)\right)^{2/3}\right] - \frac{1}{2}\left\{\left[E - V_{st} + \frac{3}{10}\left(3\pi^2\rho(r)\right)^{2/3}\right]^2 + 4\pi\rho(r)\right\}^{1/2}. \quad (20)$$

The polarization potential $V_{pol}(r)$ is taken as [37]

$$V_{pol}(r) = \begin{cases} V_{co}(r) & if\ r < r_{cp} \\ & \\ V_p(r) & if\ r \geq r_{cp} \end{cases}, \quad (21)$$

where r_{cp} is the crossing point of $V_{co}(r)$ and $V_p(r)$. For the long range, we have used polarisation potential given by, $V_p(r) = -\alpha_d/2r^4$, where α_d is the dipole polarizability of H_2S molecule and for the short range, we have chosen the following form given by Padial and Norcross [38]

$$V_{co}(r) = \begin{cases} 0.0311\ln(r_s) - 0.0584 + 0.006r_s\ln(r_s) - 0.015r_s, & r_s \leq 0.7 \\ -0.07356 + 0.02224\ln(r_s), & 0.7 \leq r_s < 10.0 \\ -0.584r_s^{-1} + 1.988r_s^{-3/2} - 2.450r_s^{-2} - 0.733r_s^{-5/2}, & r_s \geq 10.0 \end{cases} \quad (22)$$

where $r_s = [3/4\pi\rho(r)]^{1/3}$.

To consider the different inelastic channels during the scattering process, we have used the semi-empirical absorption potential $V_{abs}(r)$, expressed as [39],

$$V_{abs}(r,E) = -\rho(r)\sqrt{\frac{T_{loc}}{2}}\left(\frac{8\pi}{10k_f^3E}\right)\theta\left(k^2 - k_f^2 - 2\Delta\right)\times(A_1 + A_2 + A_3). \tag{23}$$

Here T_{loc} is the total local kinetic energy of the electron and can be represented as

$$T_{loc} = E - \left(V_{st} + V_{ex} + V_{pol}\right),$$

and $k_f = \sqrt[3]{3\pi^2\rho(r)}$ is the Fermi wave vector. $\theta(x)$ is the Pauli-blocking function. For $x \geq 0$, the value of $\theta(x)$ is unity which represents the Pauli-allowed final states of electron–H_2S collision. Otherwise, $\theta(x)$ is zero referring to the Pauli-blocked collision. A_1, A_2, A_3 are the dynamic parameters that depend upon $\theta(x)$, $\rho(r)$, E and Δ. Here Δ is the threshold parameter from where the inelastic channels open. We have taken Δ as the ionization energy of H_2S.

In the case of the positron scattering from the H_2S molecule, we have reversed the sign of the static potential as given in Equation (19) for the electron scattering case and added to it the following polarization potential given by Jain et al. [40] for the short range

$$V_{co}(r) = \begin{cases} -0.91r_s^{-1/2} + [0.00255\ \ln(r_s) - 0.0575]\ln(r_s) + 0.5835, & r_s < 0.302 \\ -0.461525 - 0.04549r_s^{-2}, & 0.302 \leq r_s < 0.56 \\ -\frac{4.3637}{(r_s+2.5)^3} + \frac{-6.5755+0.4776r_s}{(r_s+2.5)^2} + \frac{1.43275}{r_s+2.5} - 0.3149, & 0.56 \leq r_s < 8.0 \end{cases} \tag{24}$$

We have used the absorption potential given by Reid and Wadehra [41]. Its form is given as,

$$V_{ab} = 4\pi\left(\frac{a_0R}{\epsilon E_F}\right)^2\begin{cases} f(1); & \epsilon^2 - \delta \geq 1 \\ f\left(\sqrt{\epsilon^2 - \delta}\right); & 1 \geq \epsilon^2 - \delta \geq 0 \\ f(0); & 0 \geq \epsilon^2 - \delta \end{cases}. \tag{25}$$

Here, a_0 is the Bohr radius, which is taken unity and R is the Rydberg constant. $\epsilon = \sqrt{\frac{E}{E_F}}$, $\delta = \frac{\Delta(E)}{E_F}$, where E_F is the Fermi kinetic energy. $\Delta(E)$ is an important parameter for positron scattering and for absorption potential in the low to high impact energy, we chose it as proposed by Stevens et al. [48] i.e.,

$$\Delta(E) = \frac{\Delta - (\Delta - \Delta_P)}{\left[1 + (E/3I - 1)^2\right]}, \tag{26}$$

where, $\Delta_P = I - 6.8$ eV, Δ is taken as the first electronic excitation energy of H_2S molecule.

For H_2S, the required values of the dipole polarizability, ionization potential and electronic excitation energy are taken, respectively, as 24.53 a.u. [49], 10.457 eV [50] and 6.3 eV [51].

3. Results and Discussion

Through the GAUSSIAN-16 software, we have obtained the analytical form of the Gaussian wavefunction of H_2S with the STO-6G Gaussian basis set. In fact, we tested our calculation by using three basis sets viz. STO-3G, STO-4G and STO-6G wavefunctions and achieved the optimization. We obtained coefficients a_{ik} and c_{kj} and exponents α_{kj} as in Equations (10), (11) and (13) using the GAUSSIAN-16 package. The values of a_{ik} are provided in Table 1, while α_{kj} and c_{kj} are given in Table 2.

Table 1. Energy eigenvalues of the molecular orbitals of H_2S with coefficients a_{ik} as in Equation (10).

Energy Eigenvalues (eV)		**−91.82436**	**−8.62558**	**−6.31578**	**−6.31354**	**−6.31008**	**−0.88948**	**−0.50648**	**−0.39461**	**−0.28071**
	1s	0.99783	−0.35478	0.00000	−0.00731	0.00000	0.08458	0.00000	0.04775	0.00000
S	2s	0.00649	1.04753	0.00000	0.02175	0.00000	−0.28399	0.00000	−0.14345	0.00000
	$2p_x$	0.00000	0.00000	0.00000	0.00000	0.98740	0.00000	0.00000	0.00000	−0.30318
	$2p_y$	0.00000	0.00000	0.98494	0.00000	0.00000	0.00000	−0.18896	0.00000	0.00000
	$2p_z$	−0.00017	−0.01711	0.00000	0.98503	0.00000	0.05106	0.00000	−0.22009	0.00000
	3s	−0.00087	0.04782	0.00000	−0.01091	0.00000	0.79115	0.00000	0.61998	0.00000
	$3p_x$	0.00000	0.00000	0.00000	0.00000	0.04632	0.00000	0.00000	0.00000	1.03186
	$3p_y$	0.00000	0.00000	0.05717	0.00000	0.00000	0.00000	0.54074	0.00000	0.00000
	$3p_z$	0.00016	−0.00875	0.00000	0.05621	0.00000	−0.12548	0.00000	0.68194	0.00000
H1	1s	0.00021	−0.01041	−0.01140	0.01169	0.00000	0.21629	0.48298	−0.33510	0.00000
H2	1s	0.00021	−0.01041	0.01140	0.01169	0.00000	0.21629	−0.48298	−0.33510	0.00000

Table 2. Calculated values of exponents α_{kj} and coefficients c_{kj} of STO-6G orbitals of H_2S.

Atom	**Orbital**	**Exponent**	**Coefficient**
S	**1s**	0.5529038289E + 04	0.9163596281E − 02
		0.1013743118E + 04	0.4936149294E − 01
		0.2836087927E + 03	0.1685383049E + 00
		0.9742727471E + 02	0.3705627997E + 00
		0.3783386178E + 02	0.4164915298E + 00
		0.1558207360E + 02	0.1303340841E + 00
	2s	0.3455896791E + 03	−0.1325278809E − 01
		0.6840121655E + 02	−0.4699171014E − 01
		0.2125904712E + 02	−0.3378537151E − 01
		0.8179121699E + 01	0.2502417861E + 00
		0.3552198128E + 01	0.5951172526E + 00
		0.1628232301E + 01	0.2407061763E + 00
	2p	0.3455896791E + 03	0.3759696623E − 02
		0.6840121655E + 02	0.3767936984E − 01
		0.2125904712E + 02	0.1738967435E + 00
		0.8179121699E + 01	0.4180364347E + 00
		0.3552198128E + 01	0.4258595477E + 00
		0.1628232301E + 01	0.1017082955E + 00
	3s	0.1294439442E + 02	−0.7943126362E − 02
		0.3466625105E + 01	−0.7100264172E − 01
		0.1300021248E + 01	−0.1785026925E + 00
		0.5819134077E + 00	0.1510635058E + 00
		0.2879592903E + 00	0.7354914767E + 00
		0.1484042983E + 00	0.2760593123E + 00
	3p	0.1294439442E + 02	−0.7139358907E − 02
		0.3466625105E + 01	−0.1829277070E − 01
		0.1300021248E + 01	0.7621621429E − 01
		0.5819134077E + 00	0.4145098597E + 00
		0.2879592903E + 00	0.4889621471E + 00
		0.1484042983E + 00	0.1058816521E + 00
H	**1s**	0.3552322122E + 02	0.9163596281E − 02
		0.6513143725E + 01	0.4936149294E − 01
		0.1822142904E + 01	0.1685383049E + 00
		0.6259552659E + 00	0.3705627997E + 00
		0.2430767471E + 00	0.4164915298E + 00
		0.1001124280E + 00	0.1303340841E + 00

Further, we have evaluated the integral given in Equation (16) in a molecular frame of H_2S which is fixed with the S atom at (0.0000, 0.0000, 0.1030) Å and the two H atoms at the positions (0.0000, 0.9616, −0.8239) Å and (0.0000, −0.9616, −0.8239) Å as shown in Figure 1. By using these coordinates, we can obtain the values of $r_H = 2.39296$ and $r_S = 0.19464$ (in atomic unit) as required in Equation (19). The angle between the two H atoms is 92.11°.

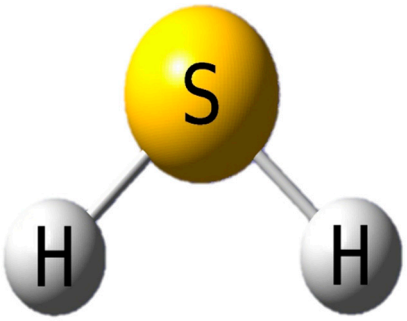


Figure 1. A diagram of C_{2v} symmetric molecule H_2S.

$\boldsymbol{r}_P$ is the product vector of the wavefunctions for H with S and two H atoms. In order that the $\boldsymbol{r}_P$ vector coincides with the molecular frame, as given in Figure 2, one must rotate $\boldsymbol{r}_P$ frame through Euler angles (α, β, γ). Here, we take $\boldsymbol{r}_P$ vector to be along the z_P axis in the r_P frame. This choice makes it possible to have the angle α = 0, which leads to significant simplifications in our geometrical considerations. Further, the direction of y_p is decided by the cross product $\boldsymbol{r}_P \times \mathbf{z}$ and the remaining axis x_p is specified to complete the standard coordinate axes. If we consider the angle between $\boldsymbol{r}_P$ and the original *z*-axis to be β, then, at first, the y_p axis is rotated by an angle β ($0 \leq \beta \leq \pi$) to bring $\boldsymbol{r}_P$ into the *z*-axis. Subsequently, the *z*-axis is rotated through angle γ so that y_p coincides with the *y*-axis of the original molecular frame. Following the above procedure of rotation, we find the Euler angles (α, β, γ) for S-H1, S-H2 and H1-H2 to be $(0, \pi - A, \pi/2)$, $(0, \pi - A, 3\pi/2)$ and $(0, \pi, \pi/2)$, respectively, where, $A = \cos^{-1}(0.694)$.

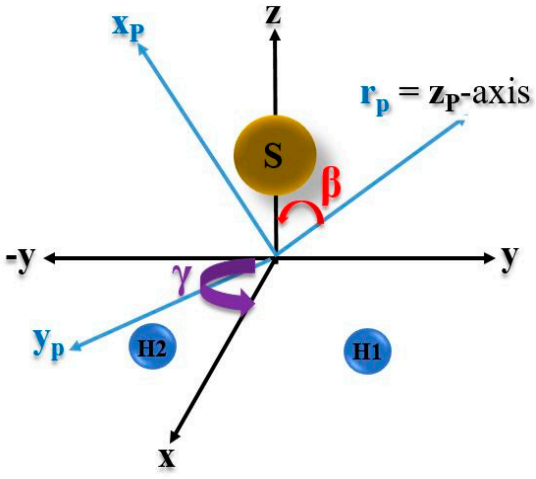


Figure 2. Diagram showing Euler angles (α, β, γ) in H_2S molecule where, (x, y, z) is the set of orthogonal vector for the fixed molecular frame. $\boldsymbol{r}_P$ is the product vector, as defined in Equation (14), while x_p is an arbitrary vector perpendicular to $\boldsymbol{r}_P$ and y_p is perpendicular to both $\boldsymbol{r}_P$ and x_p. (α, β, γ) are the standard Euler angles through which (x_p, y_p, $\boldsymbol{r}_P$) are transformed to (x, y, z).

3.1. Electron-H_2S Differential Cross Sections

We have obtained the electron impact differential cross section for H_2S in the range 15–500 eV and shown results only at a few selected energies. In Figure 3, we have shown our DCS results for

15, 20, 50, 100 eV and compared these with the available experimental results of Gulley et al. [13], Rawat et al. [14], Cho et al. [15] and Brescansin et al. [16] along with the theoretical calculations of Rawat et al. [14], Brescansin et al. [16], Varella et al. [17], Machado et al. [18] and Jain et al. [19].

For 15 eV, as shown in Figure 3a, our present calculation shows good agreement with the experimental measurement of Gulley et al. [13] up to 70°, thereafter, it slightly underestimates other results up to 120°. At the backward angles, our results show similar a nature and reasonable match with previous theoretical [17,18] calculations. It can be seen from Figure 3b that our results at 20 eV are in good agreement with both the measurements [13,15] up to 60° and then similar to other calculations [14,16–18] show two minima around 70° and 140°. Our DCSs are in better agreement with the measurements of Cho et al. [15] at the large scattering angles. Figure 3c shows that at 50 eV our results show an overall good qualitative agreement with the measured data of Brescansin et al. [16] and other theories [14,16,18,19] except for relatively sharper minima close to 55° and 135°. At 100 eV present DCSs show good agreement with measurements [14,16] till 50° and beyond that, these are slightly higher. Our results are in good agreement with the calculations of Jain et al. [19]. However, in comparison to the DCSs values from Rawat et al. [14] and Brescansin et al. [16], our results are somewhat larger, excluding the sharper minimum around 115° which is also observed by Jain et al. [19]. This is because both the calculations do not include the contribution from rotational excitation, which on the other hand, is considered in theoretical calculations of Rawat et al. [14] and Brescansin et al. [16], who showed that the sharp minimum at 100 eV disappears by including rotational excitation in calculating DCS. Since in the present calculation, we have taken the scattering from the target from a spherically averaged potential in the calculation, this might be the reason for the sharp minima which could disappear if we had considered the scattering first from the different molecular orientation and then taken the average of the results [52]. The same reason can be responsible for getting a sharper minimum around 55° for 50 eV.

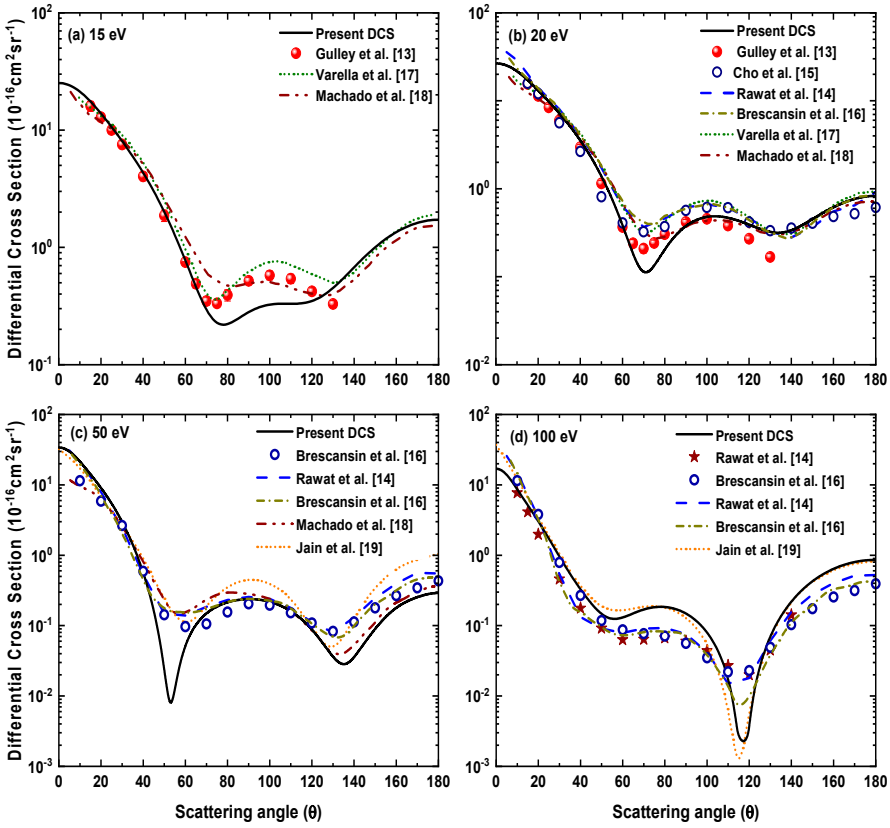


Figure 3. Differential cross sections for electron–H_2S scattering at incident electron energies (**a**) 15 eV, (**b**) 20 eV, (**c**) 50 eV and (**d**) 100 eV.

Figure 4 shows our calculated DCS results at high incident electron energies from 150–500 eV. These results have been compared with the available experimental results of Rawat et al. [14], as well as the theoretical calculations of Brescansin et al. [16], Rawat et al. [14] and Jain et al. [19]. Our DCSs show an overall reasonable agreement with both the experimental [14] and theoretical [14,16,19] results. However, the agreement among various results is better at small scattering angles. We also notice that as the energy increases, the position of minimum shifts toward the forward scattering angle. Further, as expected the backscattering decreases with the increased incident electron energy due to lesser electron–target interaction and hence, scattering is dominated in the forward direction.

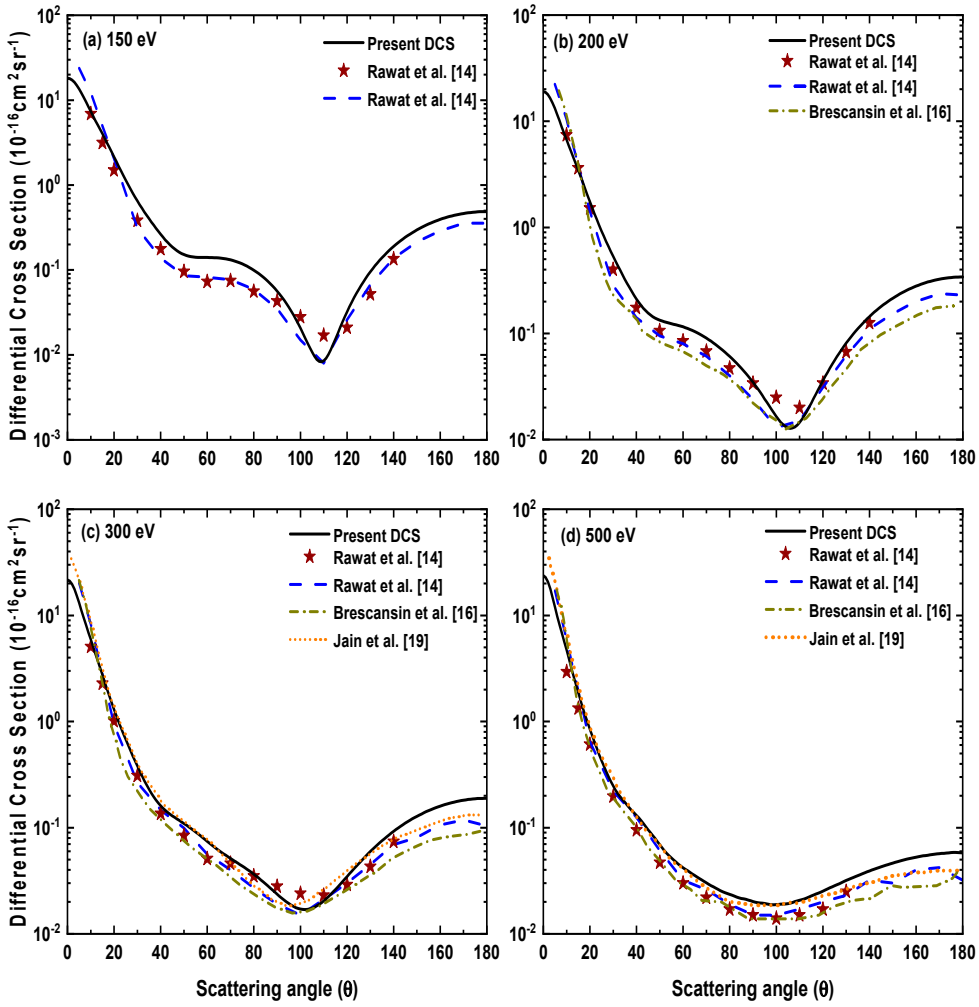


Figure 4. Differential cross sections for electron−H_2S scattering at incident electron energies (**a**) 150 eV, (**b**) 200 eV, (**c**) 300 eV and (**d**) 500 eV.

3.2. Electron-H_2S Integral and Momentum Transfer Cross Section

In Figure 5 we have compared our calculated integral and momentum transfer cross section with the experimental results of Gulley et al. [13], Rawat et al. [14], Cho et al. [15], Brescansin et al. [16] and as well as with the theoretical results of Rawat et al. [14], Brescansin et al. [16], Machado et al. [18] and Jain et al. [19]. Only measurements and calculations that have been used for comparison with our DCSs are included in Figure 5. Figure 5a shows that our ICS results are in better agreement with the measurements [13,15] in comparison to the other calculations [14,16,19], which are slightly higher up to 100 eV. The present ICSs also show good agreement with the theoretical results of Machado et al. [18]. The difference among various calculated ICSs tends to reduce beyond 100 eV. Figure 5b displays our MTCSs and their comparison with other results. As seen in the case of ICSs, the present MTCSs results

also show better agreement with the measurements of Gulley et al. [13] and Cho et al. [15] as compared to the other theoretical results [14,16,19], which overestimate the experimental cross sections up to 100 eV. All theoretical curves merge at higher energies from 100–500 eV.

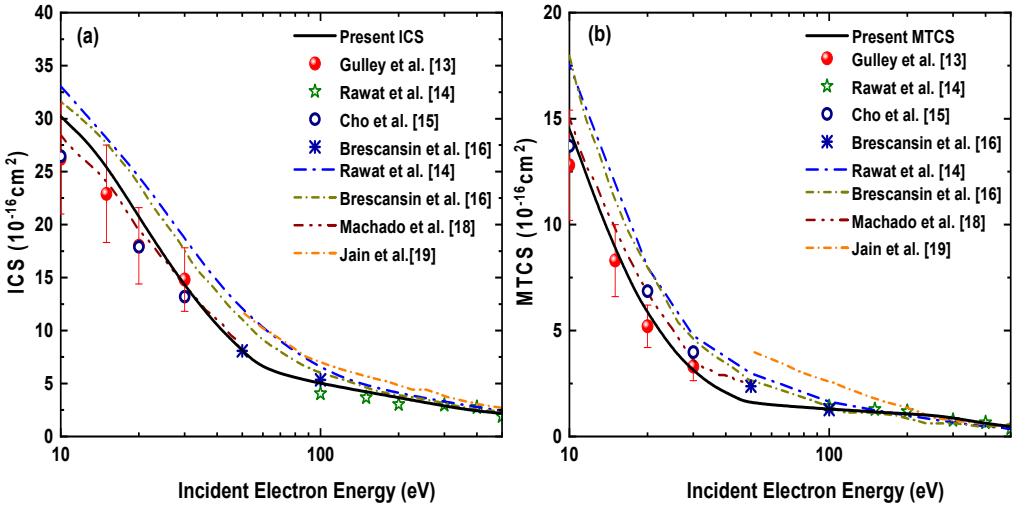


Figure 5. (**a**) Integrated cross sections and (**b**) momentum transfer cross sections for electron–H_2S elastic scattering as a function of incident electron energy.

3.3. Electron-H_2S Absorption and Total Cross Section

In Figure 6, we have shown the absorption and total cross sections with respect to the incident electron energy up to 500 eV. The present ACSs have been compared with the calculations of Brescansin et al. [16] and Jain and Baluja [25] in Figure 6a. We see that our calculated ACSs follow a similar behavior as previously reported results [16,25] in the entire energy range from ionization threshold to 500 eV. We have used the same absorption potential as taken by Brescansin et al. [16] and Jain and Baluja [25] but differ in taking a combination of the other potential components (see Equation (19)).

In Figure 6b our calculated TCSs, i.e., the total elastic cross section plus total absorption cross section, has been compared with the previous experimental measurements of Szmytkowsky et al. [26] and Zecca et al. [27] along with the theoretical results of Brescansin et al. [16], Jain and Baluja [25] and Joshipura and Vinodkumar [28].

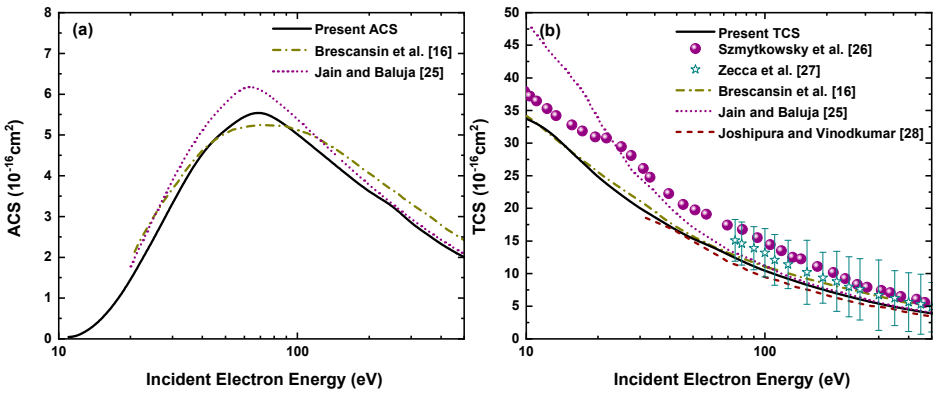


Figure 6. (**a**) Absorption cross sections and (**b**) total cross sections for electron–H_2S elastic scattering as a function of incident electron energy.

Our present TCS results are slightly lower than the experimental results of Szmytkowsky et al. [26] but lie within the error bars of the measurements reported by Zecca et al. [27]. Previously reported theoretical results [16,25,28] also show good agreement with our calculations in the entire energy range, whereas the calculations of Jain and Baluja [25] are higher at low energies but match well beyond 70 eV. Overall, our results obtained by using an analytical static potential can be said to be in good agreement with the previous measurements and calculations. In addition to the graphical display of the cross sections, we have also tabulated the present cross sections in Table 3 so that these are readily available for various possible applications.

Table 3. Cross sections for electron-H_2S scattering. The DCS is in units of 10^{-16}cm^2/sr and ICS, MTCS, ACS and TCS are in units of 10^{-16} cm^2.

	DCS							
Angle (deg)	**15 eV**	**20 eV**	**50 eV**	**100 eV**	**150 eV**	**200 eV**	**300 eV**	**500 eV**
0	25.1610	26.6501	34.0321	17.0130	18.1060	19.0440	21.5230	23.6450
5	24.1281	25.2460	29.9162	13.9210	13.5510	13.2680	13.1140	11.9590
10	21.2822	21.6572	21.4790	8.6657	7.3693	6.7151	5.9198	4.7034
15	17.5680	17.2411	14.1612	5.1474	4.0113	3.4772	2.7449	1.8663
20	13.8621	13.1460	9.0720	3.0349	2.1488	1.7617	1.2962	0.8442
30	8.0617	7.2216	2.9852	0.9611	0.6514	0.5354	0.3810	0.2470
40	4.3292	3.5418	0.5673	0.3287	0.2632	0.2117	0.1607	0.1305
50	2.0106	1.3875	0.0237	0.1466	0.1517	0.1334	0.1095	0.0689
60	0.7741	0.3847	0.0513	0.1302	0.1403	0.1156	0.0743	0.0419
70	0.2951	0.1135	0.1489	0.1692	0.1316	0.0905	0.0512	0.0302
80	0.2221	0.2033	0.2148	0.1839	0.0994	0.0608	0.0364	0.0236
90	0.2801	0.3758	0.2378	0.1484	0.0563	0.0348	0.0236	0.0201
100	0.3250	0.4784	0.2183	0.0799	0.0207	0.0165	0.0171	0.0189
110	0.3303	0.4674	0.1603	0.0174	0.0085	0.0145	0.0204	0.0207
120	0.3491	0.3908	0.0879	0.0037	0.0321	0.0358	0.0347	0.0252
130	0.4512	0.3237	0.0362	0.0692	0.0953	0.0811	0.0596	0.0318
140	0.6762	0.3374	0.0357	0.2189	0.1894	0.1444	0.0925	0.0391
150	1.0033	0.4515	0.0898	0.2462	0.2968	0.2150	0.1279	0.0464
160	1.3501	0.6156	0.1789	0.6397	0.3949	0.2796	0.1596	0.0527
170	1.6156	0.7661	0.2539	0.7997	0.4634	0.3249	0.1814	0.0569
180	1.7216	0.8306	0.2913	0.8589	0.4881	0.3415	0.1889	0.0579
ICS	25.50	20.73	8.15	4.97	4.13	3.68	2.86	2.19
MTCS	8.91	5.83	1.51	1.15	1.07	1.07	0.88	0.47
ACS	0.55	1.44	5.12	5.02	4.18	3.59	2.83	1.99
TCS	28.61	24.76	15.33	10.41	8.19	6.94	5.42	3.89

3.4. Positron-H_2S Differential Cross Section

In Figure 7, we have displayed positron impact differential cross sections for 20, 50, 100, 500 eV. So far, there are no experimental or theoretical results reported for positron—H_2S collisions with which we can compare our cross section results. From Figure 7, we notice that the position of the minima in the DCS curves move towards the forward angles as the energy increases. For the sake of comparison, in Figure 8 our DCS results for electron and positron scattering at selected energies are displayed. A clear difference in the shapes of their DCS curves can be noticed. In the case of the positron, the DCSs curves show monotonic behavior at large scattering angles, unlike electron scattering DCSs. This reveals the different nature of interactions of the two charged particles with a molecular target; for instance, exchange potential is absent in the case of the positron, while the static potential is of opposite signs for the two cases.

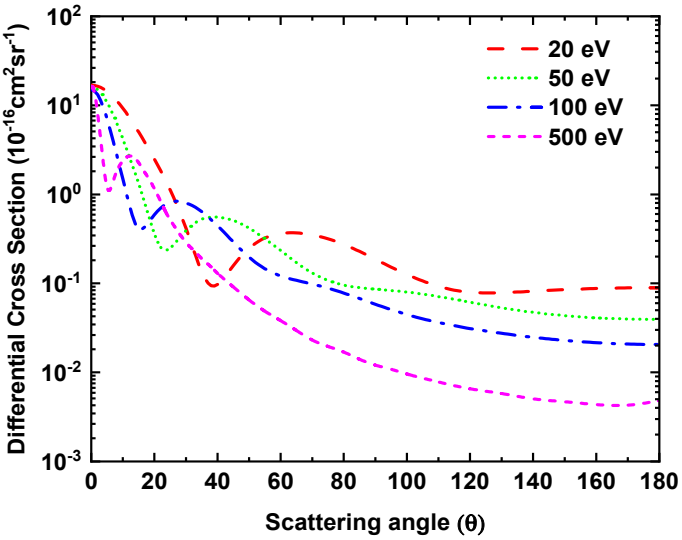


Figure 7. Differential cross sections for positron-H_2S scattering at incident positron energy 20, 50, 100 and 500 eV.

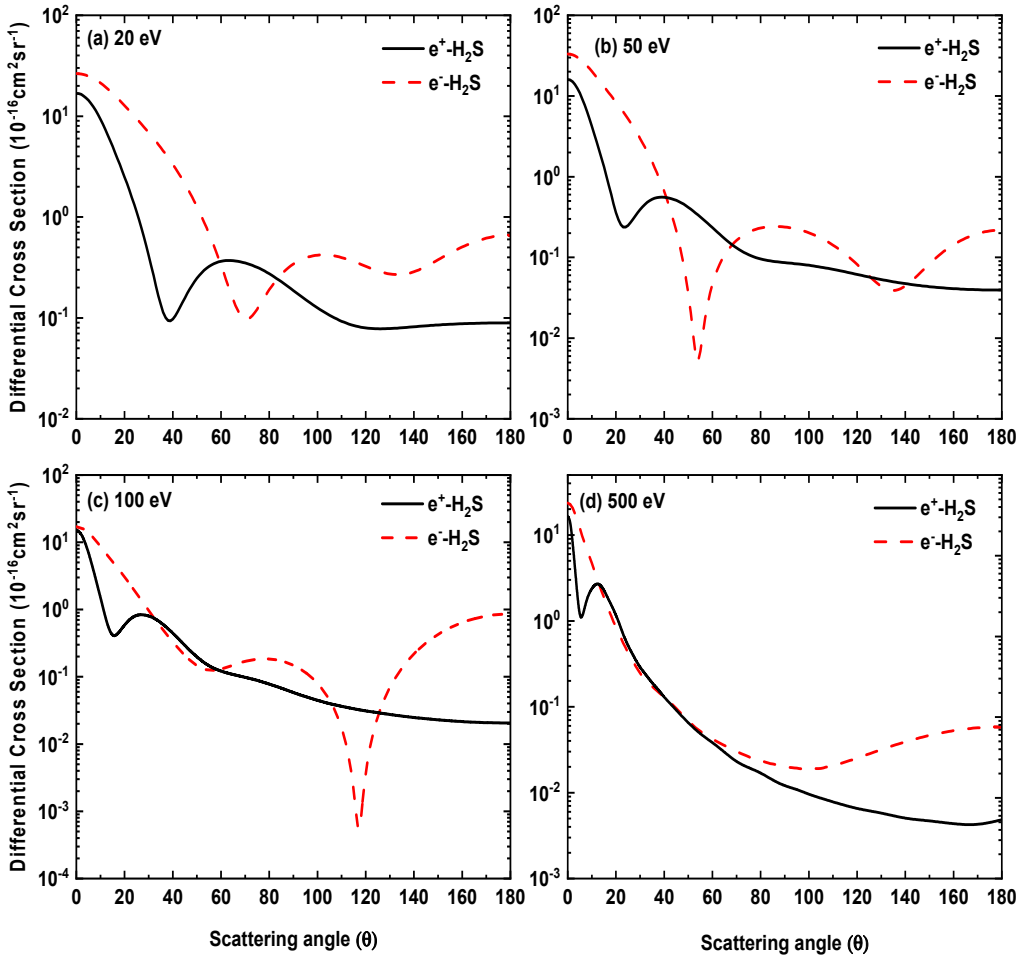


Figure 8. Comparison of differential cross sections for positron and electron scattering from H_2S at incident projectile energies (**a**) 20 eV, (**b**) 50 eV, (**c**) 100 eV and (**d**) 500 eV.

3.5. Positron-H_2S Elastic, Momentum, Absorption and Total Cross Section

Figure 9 depicts our positron impact results for elastic, momentum, absorption and total cross sections and compared these with the corresponding electron scattering cross sections.

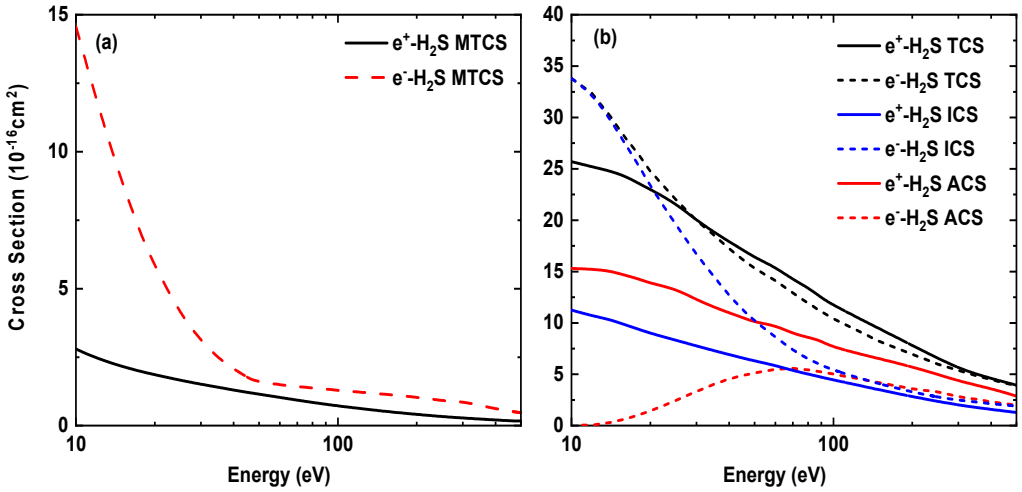


Figure 9. Comparison of cross sections for positron and electron scattering from H_2S as a function of incident projectile energy. The left graph (**a**) shows MTCSs, while the right graph (**b**) presents ICSs, ACSs and TCSs.

In Figure 9a, we can see that the momentum transfer cross sections of the positron are lower than those for the electron. These differences become smaller for energies higher than 40 eV and can be traced back to the behavior of the DCS results, which are larger for electron backward scattering. A similar feature, as found for MTCSs, can be seen for the elastic cross section results in Figure 9b. However, in the case of the absorption cross sections for positron scattering we find the opposite, i.e., these are higher than the ACSs for electron collisions in the entire energy range up to 500 eV. For the positron scattering, the inelastic channels also include the positronium formation in the ACS results. Further, we observe that the total cross sections for electron scattering are higher than the corresponding results for positron scattering up to 30 eV and the difference continues to reduce as the energy increases. This is quite expected, as with increasing energy, the polarization and exchange potentials do not influence the cross sections significantly. Since the ACSs for the positron are somewhat higher than the electrons' scattering results, we obtain slightly higher TCS results for positron scattering. The TCSs in most of the previous calculations for electron and positron scattering from other molecules [53] also show similar behaviors, i.e., the electron and positron cross sections approach each other for higher energies. Finally, all the cross sections are also provided in Table 4 for positron-H_2S elastic scattering.

Table 4. Cross sections for positron-H_2S scattering. The DCS is in units of 10^{-16}cm^2/sr and ICS, MTCS, ACS and TCS are in units of 10^{-16} cm^2.

	DCS			
Angle (deg)	**20 eV**	**50 eV**	**100 eV**	**500 eV**
0	16.7280	15.7601	15.0310	16.439
5	14.3860	10.8720	7.0699	1.0818
10	9.3056	4.2009	1.4995	2.3921
15	5.0222	1.3262	0.4113	2.2818
20	2.4881	0.3603	0.5887	1.1657
30	0.4157	0.3904	0.8018	0.2895
40	0.1007	0.5507	0.5577	0.1292
50	0.2471	0.4176	0.1975	0.0648

Table 4. *Cont.*

	DCS			
Angle (deg)	**20 eV**	**50 eV**	**100 eV**	**500 eV**
60	0.3645	0.2342	0.1214	0.0384
70	0.3504	0.1311	0.0982	0.0227
80	0.2744	0.0956	0.0778	0.0171
90	0.1868	0.0862	0.0584	0.0119
100	0.1259	0.0799	0.0447	0.0095
110	0.0927	0.0711	0.0364	0.0078
120	0.0796	0.0616	0.0311	0.0064
130	0.0785	0.0532	0.0275	0.0059
140	0.0817	0.0472	0.0248	0.0049
150	0.0852	0.0434	0.0229	0.0047
160	0.0870	0.0416	0.0219	0.0043
170	0.0889	0.0398	0.0208	0.0041
180	0.0893	0.0394	0.0206	0.0048
ICS	9.01	6.30	4.45	1.28
MTCS	1.86	1.15	0.72	0.17
ACS	14.03	10.09	7.24	2.66
TCS	23.04	16.39	11.69	3.94

4. Conclusions

In the present work, we have analytically calculated spherically averaged static potential to study the electron and positron impact elastic scattering from hydrogen sulfide, using the complex optical model potential approach. Along with the static potential, exchange, polarization and absorption potentials are also considered in our calculations. The target H_2S is represented by STO-6G basis set to calculate the charge density and subsequently, the static potential. We obtained Euler angles for calculating the overlap integrals involving the product of orbital wavefunctions of one atom with another in a particular molecular frame. Solving integrals in this manner makes our method unique in comparison to the other existing theoretical techniques. We have reported the results for DCS for electron and positron impact energies from 20–500 eV along with ICS, MTCS, ACS and TCS from 10–500 eV. All our reported results for electron scattering are compared with the available other theoretical and experimental results and we observed overall a good agreement. For positron scattering, we reported the cross section results for the first time and compared them with the electron scattering cross sections to study the difference between the two cases. We found that the total cross sections for electron and positron impact differ at lower energies. Thereafter, both the cross sections are very close to each other, as expected and noticed in most previous studies on other molecules. From our present study, we can say that we have presented a successful application of our technique of using the analytical static potential to describe electron and positron elastic collision with H_2S and the same can be further extended to study bigger and more complex molecules as well.

Author Contributions: D.M. performed the cross section calculations. D.M., L.S. and R.S. contributed in the research discussion and writing the manuscript. All authors have read and agreed to the published version of the manuscript.

Funding: At present we have not received any external funding.

Acknowledgments: D.M. is grateful to the Ministry of Human Resources and Development (MHRD) India for the award of research and teaching assistantship. R.S. and L.S. are thankful to the CSIR for the sanction of research project to carry this work.

Conflicts of Interest: The authors declare no conflict of interest.

References

1. Bockelée-Morvan, D.; Colom, P.; Crovisier, J.; Despois, D.; Paubert, G. Microwave detection of hydrogen sulphide and methanol in comet Austin (1989c1). *Nature* **1991**, *350*, 318–320. [CrossRef]
2. Irwin, P.G.J.; Toledo, D.; Garland, R.; Teanby, N.A.; Fletcher, L.N.; Orton, G.A.; Bézard, B. Detection of hydrogen sulfide above the clouds in Uranus's atmosphere. *Nat. Astron.* **2018**, *2*, 420–427. [CrossRef]
3. Phuong, N.T.; Chapillon, E.; Majumdar, L.; Dutrey, A.; Guilloteau, S.; Piétu, V.; Wakelam, V.; Diep, P.N.; Tang, Y.-W.; Beck, T.; et al. First detection of H_2S in a protoplanetary disk. *Astron. Astrophys.* **2018**, *616*, L5. [CrossRef]
4. Chupp, E.L.; Forrest, D.J.; Higbie, P.R.; Suri, A.N.; Tsai, C.; Dunphy, P.P. Solar Gamma Ray Lines observed during the Solar Activity of August 2 to August 11, 1972. *Nature* **1973**, *241*, 333–335. [CrossRef]
5. Leventhal, M.; MacCallum, C.J.; Stang, P.D. Detection of 511 keV positron annihilation radiation from the galactic center direction. *Astrophys. J.* **1978**, *225*, L11–L14. [CrossRef]
6. Trajmar, S.; Register, D.F.; Chutjian, A. Electron scattering by molecules II. Experimental methods and data. *Phys. Rep.* **1983**, *97*, 219–356. [CrossRef]
7. Wang, R.; Fan, Q.; Zhang, J.; Zhang, X.; Kang, Y.; Wang, Z. Hydrogen Sulfide Demonstrates Promising Antitumor Efficacy in Gastric Carcinoma by Targeting MGAT5 1,2. *Transl. Oncol.* **2018**, *11*, 900–910. [CrossRef]
8. Wen, Y.-D.; Wang, H.; Zhu, Y.-Z. The Drug Developments of Hydrogen Sulfide on Cardiovascular Disease. *Oxid. Med. Cell. Longev.* **2018**, *2018*, 4010395. [CrossRef]
9. Agostinelli, S.; Allison, J.; Amako, K.; Apostolakis, J.; Araujo, H.; Arce, P.; Asai, M.; Axen, D.; Banerjee, S.; Barrand, G.; et al. GEANT4—A simulation toolkit. *Nucl. Instrum. Methods Phys. Res. Sect. A* **2003**, *506*, 250–303. [CrossRef]
10. Baró, J.; Sempau, J.; Fernández-Varea, J.M.; Salvat, F. PENELOPE: An algorithm for Monte Carlo simulation of the penetration and energy loss of electrons and positrons in matter. *Nucl. Instrum. Methods Phys. Res. B* **1995**, *100*, 31–46. [CrossRef]
11. Blanco, F.; Muñoz, A.; Almeida, D.; da Silva, F.F.; Limão-Vieira, P.; Fuss, M.C.; Sanz, A.G.; García, G. Modelling low energy electron and positron tracks in biologically relevant media. *Eur. Phys. J. D* **2013**, *67*, 199. [CrossRef]
12. Ruset, C.; Bloyce, A.; Bell, T. Plasma nitrocarburising with nitrogen, hydrogen, and hydrogen sulphide gas mixtures. *Surf. Eng.* **1995**, *11*, 308–314. [CrossRef]
13. Gulley, R.J.; Brunger, M.J.; Buckman, S.J. The scattering of low energy electrons from hydrogen sulphide. *J. Phys. B At. Mol. Opt. Phys.* **1993**, *26*, 2913–2925. [CrossRef]
14. Rawat, P.; Iga, I.; Lee, M.-T.; Brescansin, L.M.; Homem, M.G.P.; Machado, L.E. Cross sections for elastic electron–hydrogen sulfide collisions in the low- and intermediate-energy range. *Phys. Rev. A* **2003**, *68*, 052711. [CrossRef]
15. Cho, H.; Park, S.J.; Park, Y.S. Measurements of elastic electron scattering by hydrogen sulfide extended to backward angles. *J. Korean Phys. Soc.* **2005**, *46*, 431–434.
16. Brescansin, L.M.; Machado, L.E.; Lee, M.-T.; Cho, H.; Park, Y.S. Absorption effects in intermediate-energy electron scattering by hydrogen sulphide. *J. Phys. B At. Mol. Opt. Phys.* **2008**, *41*, 185201. [CrossRef]
17. Varella, M.T.d.N.; Bettega, M.H.F.; Lima, M.A.P.; Ferreira, L.G. Low-energy electron scattering by H_2O, H_2S, H_2Se, and H_2Te. *J. Chem. Phys.* **1999**, *111*, 6396–6406. [CrossRef]
18. Machado, L.E.; Leal, E.P.; Mu-Tao, L.; Brescansin, L.M. Low energy elastic scattering of electrons by hydrogen sulphide molecules. *J. Mol. Struct. THEOCHEM* **1995**, *335*, 37–43. [CrossRef]
19. Jain, A.K.; Tripathi, N.; Jain, A. Elastic scattering ofelectrons by H_2S at 50—1000 eV. *Phys. Rev. A* **1990**, *42*, 6912–6915. [CrossRef]
20. Gianturco, F.A. Ab initio model calculations to treat electron scattering from polar polyatomic targets: H_2S and NH_3. *J. Phys. B At. Mol. Opt. Phys.* **1991**, *24*, 4627–4648. [CrossRef]
21. Yuan, J.; Zhang, Z. Electron scattering with H_2S and PH_3 molecules. *Zeitschrift Für Phys. D Atoms Mol. Clust.* **1993**, *28*, 207–214. [CrossRef]
22. Nishimura, T.; Itikawa, Y. Vibrationally elastic and inelastic scattering of electrons by hydrogen sulphide molecules. *J. Phys. B At. Mol. Opt. Phys.* **1996**, *29*, 4213–4226. [CrossRef]

23. Gupta, M.; Baluja, K.L. Application of R-matrix method to electron-H_2S collisions in the low energy range. *Eur. Phys. J. D* **2007**, *41*, 475–483. [CrossRef]
24. Aouchiche, H.; Medegga, F.; Champion, C. Doubly differential and integral cross sections for electron elastic scattering by hydrogen sulfide. *Nucl. Instrum. Methods Phys. Res. Sect. B Beam Interact. Mater. Atoms* **2014**, *333*, 113–119. [CrossRef]
25. Jain, A.; Baluja, K.L. Total (elastic plus inelastic) cross sections for electron scattering from diatomic and polyatomic molecules at 10—5000 eV: H_2, Li_2, HF, CH_4, N_2, CO, C_2H_2, HCN, O_2, HC1, H_2S, PH_3, SiH_4, and CO_2. *Phys. Rev. A* **1992**, *45*, 202–218. [CrossRef]
26. Szmytkowski, C.; Mozejko, P.; Krzysztofowicz, A. Measurements of absolute total cross sections for electron scattering from triatomic polar molecules: SO_2 and H_2S. *Radiat. Phys. Chem.* **2003**, *68*, 307–311. [CrossRef]
27. Zecca, A.; Karwasz, G.P.; Brusa, R.S. Total-cross-section measurements for electron scattering by NH_3, SiH_4, and H_2S in the intermediate-energy range. *Phys. Rev. A* **1992**, *45*, 2777–2783. [CrossRef]
28. Joshipura, K.N.; Vinodkumar, M. Total cross sections of electron collisions with S atoms; H_2S, OCS and SO_2 molecules (E i $\geq$ 50 eV). *Z. Phys. D* **1997**, *41*, 133–137. [CrossRef]
29. Limbachiya, C.; Vinodkumar, M.; Mason, N. Calculation of electron-impact rotationally elastic total cross sections for NH_3, H_2S, and PH_3 over the energy range from 0.01 eV to 2 keV. *Phys. Rev. A* **2011**, *83*, 042708. [CrossRef]
30. Joachain, C.J. *Quantum Collision Theory*, 3rd ed.; North Holland: Amsterdam, The Netherlands, 1983.
31. Schiff, L.I. *Quantum Mechanics*, 3rd ed.; Tata McGraw-Hill: New York, NY, USA, 2010.
32. Milisavljević, S.; Šević, D.; Chauhan, R.K.; Pejčev, V.; Filipović, D.M.; Srivastava, R.; Marinković, B.P. Differential and integrated cross sections for the. *J. Phys. B At. Mol. Opt. Phys.* **2005**, *38*, 2371–2384. [CrossRef]
33. Tennyson, J. Electron-molecule collision calculations using the R-matrix method. *Phys. Rep.* **2010**, *491*, 29–76. [CrossRef]
34. Gianturco, F.A.; Jain, A. The theory of electron scattering from polyatomic molecules. *Phys. Rep.* **1986**, *143*, 347–425. [CrossRef]
35. Sanna, N.; Baccarelli, I.; Morelli, G. SCELib3.0: The new revision of SCELib, the parallel computational library of molecular properties in the Single Center Approach. *Comput. Phys. Commun.* **2009**, *180*, 2544–2549. [CrossRef]
36. Gianturco, F.A.; Scialla, S. Local approximations of exchange interaction in electron-molecule collisions: The methane molecule. *J. Phys. B At. Mol. Phys.* **1987**, *20*, 3171–3189. [CrossRef]
37. O'Connell, J.K.; Lane, N.F. Nonadjustable exchange-correlation model for electron scattering from closed-shell atoms and molecules. *Phys. Rev. A* **1983**, *27*, 1893–1903. [CrossRef]
38. Padial, N.T.; Norcross, D.W. Parameter-free model of the correlation-polarization potential for electron-molecule collisions. *Phys. Rev. A* **1984**, *29*, 1742–1748. [CrossRef]
39. Staszewska, G.; Schwenke, D.W.; Thirumalai, D.; Truhlar, D.G. Quasifree-scattering model for the imaginary part of the optical potential for electron scattering. *Phys. Rev. A.* **1983**, *28*, 2740–2751. [CrossRef]
40. Jain, A. Low-energy positron-argon collisions by using parameter-free positron correlation polarization potentials. *Phys. Rev. A* **1990**, *41*, 2437–2444. [CrossRef]
41. Reid, D.D.; Wadehra, J.M. A quasifree model for the absorption effects in positron scattering by atoms. *J. Phys. B At. Mol. Opt. Phys.* **1996**, *29*, L127–L133. [CrossRef]
42. Bransden, B.H.; Joachain, C.J. *Physics of Atoms and Molecules*, 2nd ed.; Prentice Hall Pearson: Upper Saddle River, NJ, USA, 2003.
43. Das, T.; Stauffer, A.D.; Srivastava, R. A method to obtain static potentials for electron-molecule scattering. *Eur. Phys. J. D* **2014**, *68*, 102. [CrossRef]
44. Mahato, D.; Sharma, L.; Stauffer, A.D.; Srivastava, R. Electron impact elastic scattering from methane and silane molecules. *Eur. Phys. J. D* **2019**, *73*, 189. [CrossRef]
45. Mahato, D.; Sharma, L.; Srivastava, R. An approach to study electron and positron scattering from NH_3 and PH_3 using the analytic static potential. *J. Phys. B At. Mol. Opt. Phys.* **2020**, *53*, 225204. [CrossRef]
46. Tóth, I.; Campeanu, R.I.; Chiş, V.; Nagy, L. Screening effects in the ionization of molecules by positrons. *Phys. Lett. A* **2006**, *360*, 131–134. [CrossRef]
47. Tóth, I.; Campeanu, R.I.; Nagy, L. Ionization of NH_3 and CH_4 by electron impact. *Eur. Phys. J. D* **2015**, *69*, 2. [CrossRef]

48. Stevens, D.; Babij, T.J.; Machacek, J.R.; Buckman, S.J.; Brunger, M.J.; White, R.D.; García, G.; Blanco, F.; Ellis-Gibbings, L.; Sullivan, J.P. Positron scattering from pyridine. *J. Chem. Phys.* **2018**, *148*, 144308. [CrossRef]
49. Olney, T.N.; Cann, N.M.; Cooper, G.; Brion, C.E. Absolute scale determination for photoabsorption spectra and the calculation of molecular properties using dipole sum-rules. *Chem. Phys.* **1997**, *223*, 59–98. [CrossRef]
50. Lias, S.G. *NIST Chemistry WebBook, NIST Standard Reference Database Number 69*; National Institute of Standards and Technology: Gaithersburg, MD, USA, 2020.
51. Lidez, D.R. *CRC Handbook of Physics and Chemistry*, 74th ed.; Chemical Rubber Company, Ed.; CRC Press: Boca Raton, FL, USA, 1993.
52. Da Paixo, F.J.; Lima, M.A.P.; McKoy, V. Spin exchange in elastic e-O_2 collisions. *Phys. Rev. Lett.* **1992**, *68*, 1698–1701. [CrossRef]
53. Makochekanwa, C.; Sueoka, O.; Kimura, M. Similarities and differences between electron and positron scattering from molecules. *J. Phys. Conf. Ser.* **2007**, *80*, 012012. [CrossRef]

Publisher's Note: MDPI stays neutral with regard to jurisdictional claims in published maps and institutional affiliations.

© 2020 by the authors. Licensee MDPI, Basel, Switzerland. This article is an open access article distributed under the terms and conditions of the Creative Commons Attribution (CC BY) license (http://creativecommons.org/licenses/by/4.0/).